IJL, Vol. 25, Issue 1, 2026
http://doi.org/10.31900/ijl.v25i1.581

Research Article

IRAQI JOURNAL OF LASER

The Effect of Fe Doping on the Structural and Optical Properties of (CuO:ZnO) Thin Films Prepared by the PLD Technique

Rusul R. Alrubaye* and Ghuson H. Mohammed

Department of Physics, College of Science, University of Baghdad, Iraq
**Email address of the Corresponding Author: Rusul.Abd2404m@sc.uobaghdad.edu.iq*

Article history: Received 12 May. 2025, Accepted 10 Dec. 2025, Published online 15 Jun. 2026

Abstract: This study investigates the structural and optical properties of Fe-doped (CuO: ZnO) thin films with varying Fe contents (x = 0.1–0.5%) deposited on glass substrates via pulsed laser deposition (PLD) at ambient temperature under a vacuum of 1×10^{-2} mbar. X-ray diffraction (XRD) confirmed that all films maintained a monoclinic polycrystalline structure, with grain size decreasing with increasing Fe concentration. Energy Dispersive X-ray Spectroscopy (EDS) verified the successful incorporation of Fe without altering the Cu and Zn composition. Increasing Fe concentration significantly affected the optical transmission, absorption, refractive index (n), extinction coefficient (k), and dielectric constants, demonstrating that Fe doping strongly modifies the structural, optical, and dielectric properties of CuO: ZnO thin films.

Keywords: CuO: ZnO Thin Films, PLD, XRD, Nd:YAG laser, and structural properties.

1. Introduction

Transition metal oxides (TMOs), such as CuO, ZnO, TiO_2, and NiO, represent an important class of semiconductors widely employed in electronics, catalysis, and solar energy conversion [1]. These oxides exhibit excellent energy storage capabilities and possess notable functional properties, including chemical stability, biocompatibility, and pressure and gas-sensitivity, making them suitable for a wide range of practical applications [2]. Among TMOs, copper oxide semiconductors have been extensively studied due to their unique structural and optical properties. Two stable forms of copper oxide, CuO and Cu_2O, exhibit distinct differences in colour, crystal structure, and physical properties. TMOs, including CuO and ZnO, are commonly used as functional components in photovoltaic devices, serving as absorbing layers, electron transport layers, transparent conducting electrodes, and photoanodes [3]. CuO exhibits exceptionally high melting and boiling points, making it one of the most thermally stable materials. Its monoclinic crystal structure, intrinsically stable direct band gap (E_g = 1.2–1.9 eV), and the presence of negatively charged copper vacancies acting as acceptors classify CuO as an inherent p-type semiconductor. Owing to its outstanding visible-range absorption properties, CuO is a promising candidate as an active layer in photovoltaic and solar cell applications [4, 5]. Furthermore, CuO can be synthesized using cost-effective solution-based methods and possesses several advantageous properties, including non-toxicity, chemical

stability, electrochemical activity, and the abundance of readily available raw materials [6]. Copper oxide has been extensively studied due to its suitability for a wide range of practical applications, including micro-electromechanical systems, spintronics, solar cells, and gas sensors [7]. High surface-to-volume CuO nanostructures exhibit unique chemical and physical properties, making them useful in biosensors, supercapacitors, photodetectors, solar cells, and catalysis [8]. Zinc oxide (ZnO), another semiconductor, is widely used in the fabrication of photovoltaic solar cells [9]. ZnO is safe, easy to synthesize, and exhibits strong light absorption. Because it has a direct band gap, ZnO behaves as a p-type semiconductor, with an indirect band gap of 1–1.8 eV, which is nearly ideal for solar cells and helps it absorb sunlight effectively [10]. Doping with Fe significantly affects the magnetic and electrical properties of these semiconductors [11].

In addition to modifying the material dimensions, Fe doping influences multiple physical and chemical properties, yielding materials with enhanced functional characteristics [12]. Several methods have been employed to fabricate CuO thin films, including thermal oxidation of Cu films [13], reactive DC sputtering [14], sol-gel spin coating [15], RF magnetron sputtering [16], and spray pyrolysis [17]. Pulsed laser deposition is particularly advantageous due to its simplicity, scalability, environmental friendliness, and precise control over composition and film thickness. Many studies have been conducted in recent years to develop the structural and optical properties of copper oxide (CuO) using various techniques to improve its performance in electronic and optical applications. Borah and Sarma's study showed that films prepared using continuous magnetron sputtering exhibit omnidirectional structures with grain sizes up to 26 nm. They also demonstrated that reducing the sputtering pressure increases light absorption in the 280–400 nm range and improves optical transmittance by 80% [18]. Meanwhile, Abeer and Jamal prepared thin films of CuO and CuO mixed with Nd_2O_3 using pulsed laser deposition for ammonia gas sensing. The results showed that adding Nd_2O_3 altered the crystal structure, reducing the crystal size from 19 nm to 14.7 nm, and significantly improved the optical properties [19].

Furthermore, Soumen et al.'s study, which used a simple chemical method to prepare CuO nanotubes, showed that the prepared samples possessed a monoclinic structure with a band gap ranging between (2.86-2.89 eV), where these structures showed distinct photocatalytic activity in the decomposition of methylene blue dye [20]. Abeer and Jamal's study also showed that mixing lanthanum oxide (La_2O_2) with (CuO) prepared by the PLD method contributes to increasing the band gap from (2.25) to (2.85), which confirms the possibility of modifying the structural and optical properties of (CuO) through its combination with different oxides [21]. Based on the above, these studies clearly show that the properties of (CuO) are greatly affected by the type of doping and the method of preparation. However, the effect of the iron element in the composite system (CuO: ZnO) prepared by pulsed laser deposition purification has not been systematically and in-depth studied, which represents a clear research gap that deserves investigation. Hence, the importance of this study lies in providing a detailed description of the effects of different iron concentrations on the structural and optical properties of (CuO: ZnO) films prepared by PLD, while also demonstrating the relationships among crystal structure, energy gap, and optical absorption behaviour. This aims to improve the performance of these films, making them promising materials for optical and electronic applications such as solar cells and high-efficiency sensors.

2. Experimental

The deposition process was carried out using varying concentrations of cast iron (Fe) ranging from 0.1 - 0.5% weight percentages, added to an equivalent mixture of copper oxide (CuO) and zinc oxide (ZnO). The materials were then homogeneously mixed by mechanical separation to ensure a uniform distribution of iron particles. The resulting powder was then pressed 8 tons for 10 minutes using a hydraulic press, forming discs with a diameter of 1 cm and a thickness of 1 cm. These discs were then heated at 300°C for one hour

and allowed to cool to room temperature. The discs were subsequently placed in a pulsed laser deposition chamber to deposit a film on pre-cleaned glass substrates using a mixture of salt and alcohol, followed by ultrasonic testing for 15 minutes. A pulsed Nd: YAG laser with a fundamental wavelength of 1064 nm was used, with a pulse energy of 600 mJ, a repetition rate of 6 Hz, and a spot diameter of 4 mm. The laser beam was tilted at a 45° angle to the target surface, with 400 pulses. The chamber pressure was maintained at a constant 1×10^{-2} mbar, and the distance between the laser nozzle and the target was kept at 2 cm. The resulting film thickness was approximately 200 ± 5 nm. Structural analyses were performed using X-ray diffraction within an angular range of 10°–80° with Cu-Kα radiation at a wavelength of 0.154 nm. Optical properties were measured by spectroscopy over 340–1100 nm. Figure 1 shows a diagram illustrating the pulsed laser deposition system.

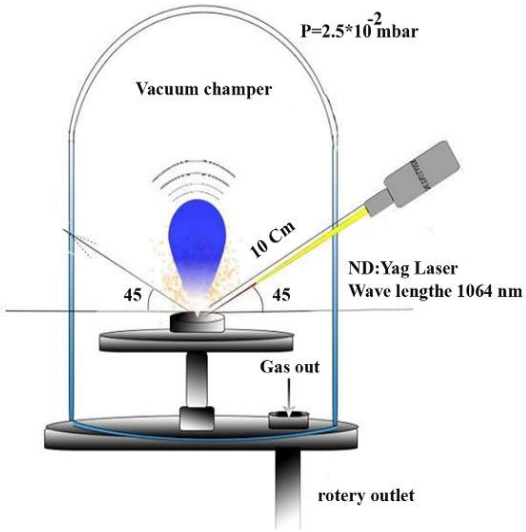

Fig. 1: Schematic illustration of the pulsed laser deposition system.

3. Result and discussion

3.1 X-ray diffraction analysis

The crystal structure of $(CuO: Zn)_{1-x}(Fe)_x$ thin films was analyzed using XRD within the 2θ range of 20°–80°. Figure 2 presents the XRD patterns of the (CuO: ZnO) Fe thin films with varying Fe concentrations. The diffraction patterns exhibit multiple peaks for all samples, confirming the polycrystalline nature of the deposited films. Four peaks were observed at 32.76°, 38.77°, 61.66°, and 66.06°, corresponding to the (110), (11–1), (111), and (–113) planes, respectively, with a preferred orientation along the (11–1) plane. These peaks can be indexed to the monoclinic structure of CuO and match well with JCPDS card No. 48-1548. Several less intense peaks were detected at 31.83°, 34.37°, and

36.45°, corresponding to the (100), (002), and (101) planes of ZnO, in agreement with JCPDS card No. 36-1451. The diffraction spectra confirm the successful crystallization of the CuO nanostructures within the deposited films. The Fe-doped films did not exhibit any secondary phases or additional peaks associated with Fe compounds. The absence of Fe-related peaks in the XRD patterns suggests that Fe ions were successfully incorporated into the CuO lattice by substituting Cu^{+} sites rather than forming separate phases. This observation indicates that the crystal structure of CuO remained stable upon Fe incorporation, confirming the successful substitution of Fe^{+} ions into the host lattice [22].

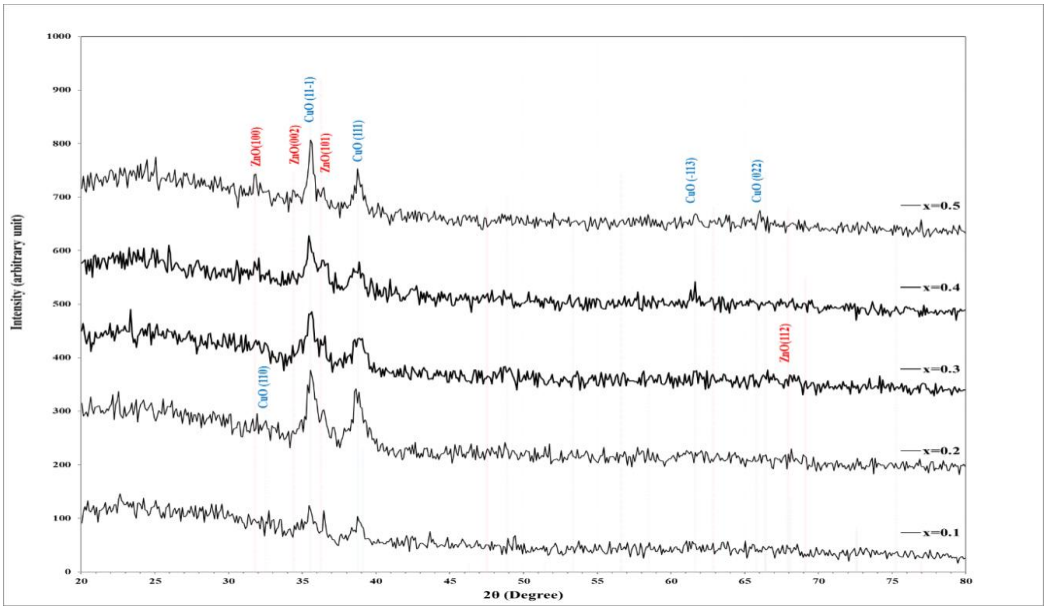

Fig.2: XRD diffraction pattern of Fe-doped CuO: ZnO thin films for different Fe content.

Scherrer's equation was used to determine and quantify the average crystallite size (L) as follows in Eq. (1), [23]:

$$L = K\lambda/\beta.\cos\theta \quad (1)$$

Where λ denotes the XRD wavelength in nanometers (nm), the value of β is the diffraction peak profile's peak width at half maximum height in radians. K is the shape factor, which is typically taken to be 0.89 for ceramic materials and, θ is the diffracted angle of the peak.

The interplanar spacing (d_{hkl}) was calculated using Bragg's law as follows in Eq. (2):

$$n\,\lambda = 2d_{hkl}\sin\theta_B \quad (2)$$

Where (θ_B) is Bragg's angle, λ is the X-ray wavelength, n is an integer representing the diffraction order (1, 2, etc.), and d_{hkl} is the interplanar spacing between two successive planes. The interplanar spacing for the samples was listed in Table 1.

The lattice constant (a) was also calculated from Eq. (3) and illustrated in Table 1.

$$\frac{1}{d^2} = \frac{h^2+k^2+l^2}{a^2} \quad (3)$$

Where (hkl) are miller indices.

The stability of the crystal structure of iron-doped (CuO: ZnO) films can be attributed to the ionic compatibility between Fe^{2+} and Cu^{2+} ions in the crystal lattice. This facilitates molecular substitution without causing significant structural distortions. It is believed that the introduction of iron into the copper sites improves intergranular bonding and reduces the density of crystal defects, which explains the appearance of the preferred orientation pattern at the (11-1) plane. The absence of additional phases further confirms that the doping did not cause chemical separation but merely stabilized the parent structure and improved its structural and optical properties.

Table 1. Structural parameters of Fe-doped CuO: ZnO thin films.

x	2θ (Deg.)	FWHM (Deg.)	d_{hkl} (Å)	D (nm)	Phase	hkl	δ ×10¹⁵ (line/m²)	ε
0.1	32.7620	0.5576	2.7313	14.9	CuO	(110)	4.5346	0.0083
	35.4569	0.6814	2.5297	12.2	CuO	(11-1)	6.6747	0.0093
	36.4481	0.4647	2.4631	18.0	ZnO	(101)	3.0870	0.0062
	38.7713	0.8364	2.3207	10.1	CuO	(111)	9.8633	0.0104
0.2	32.5452	0.5886	2.7490	14.1	CuO	(110)	5.0585	0.0088
	35.5808	0.7125	2.5211	11.7	CuO	(11-1)	7.2929	0.0097
	36.4481	0.5885	2.4631	14.2	ZnO	(101)	4.9509	0.0078
	38.6164	0.7124	2.3297	11.8	CuO	(111)	7.1623	0.0089
0.3	32.4832	0.4337	2.7717	12.8	CuO	(110)	6.1319	0.0098
	35.5498	0.7744	2.5238	19.8	CuO	(11-1)	2.5455	0.0057
	38.8023	0.9912	2.3277	21.7	CuO	(111)	2.1307	0.0048
0.4	31.9257	0.5886	2.8009	14.0	CuO	(110)	5.0743	0.0090
	35.4879	0.7434	2.5275	11.2	CuO	(11-1)	7.9433	0.0101
	36.5101	0.7434	2.4591	11.3	ZnO	(101)	7.3974	0.0098
	38.7093	0.8674	2.3243	9.7	CuO	(111)	10.6120	0.0108
	61.6004	0.5575	1.5044	16.6	CuO	(-113)	3.6335	0.0041
0.5	31.8327	0.6195	2.8089	13.3	ZnO	(110)	5.6237	0.0095
	34.3727	0.5575	2.6069	14.9	ZnO	(002)	4.4947	0.0079
	35.5498	0.4646	2.5233	18.0	CuO	(11-1)	3.1014	0.0063
	36.2932	0.5886	2.4733	14.2	ZnO	(101)	4.9570	0.0078
	38.7403	0.8363	2.3225	10.1	CuO	(111)	9.8628	0.0104
	61.6624	0.5886	1.5030	15.7	CuO	(-113)	4.0476	0.0043
	66.0609	0.5266	1.4132	18.0	CuO	(022)	3.0884	0.0035

3.2 Energy Dispersive X-ray Spectroscopy (EDS) analysis

Energy-Dispersive X-ray Spectroscopy (EDS) was performed to examine the effect of Fe incorporation on the elemental composition of the prepared films. Figure 3 presents the comparative EDS spectra obtained before and after Fe doping, highlighting changes in the intensities of Fe, Cu, and Zn peaks. Before the incorporation of Fe, the EDS spectrum exhibited prominent characteristic peaks corresponding to copper (Cu Kα ≈ 8.04 keV) and zinc (Zn Kα ≈ 8.63 keV), along with minor peaks from other trace elements. No detectable signals were observed in the energy range associated with Fe, and upon introducing a small fraction of Fe, a distinct new peak appeared at approximately 6.40 keV, corresponding to the Fe Kα line, providing qualitative confirmation of Fe incorporation into the film. The Fe Kβ line (≈ 7.06 keV The Fe Kβ line (≈ 7.06 keV) was not observed, which is expected due to the low Fe concentration and the inherently weaker intensity of the Kβ transition relative to Kα.

Notably, the intensities of Cu and Zn peaks remained nearly unchanged after Fe addition. The appearance of the Fe peak, without significant alteration in Cu and Zn intensities, indicates that Fe acted as a minor dopant incorporated into the CuO: ZnO lattice rather than substituting or diminishing the primary

constituent elements. Additional weak peaks of silicon and oxygen were also detected, originating from the underlying glass substrate. These results further confirm the successful and homogeneous incorporation of Fe within the host matrix, in good agreement with the XRD findings.

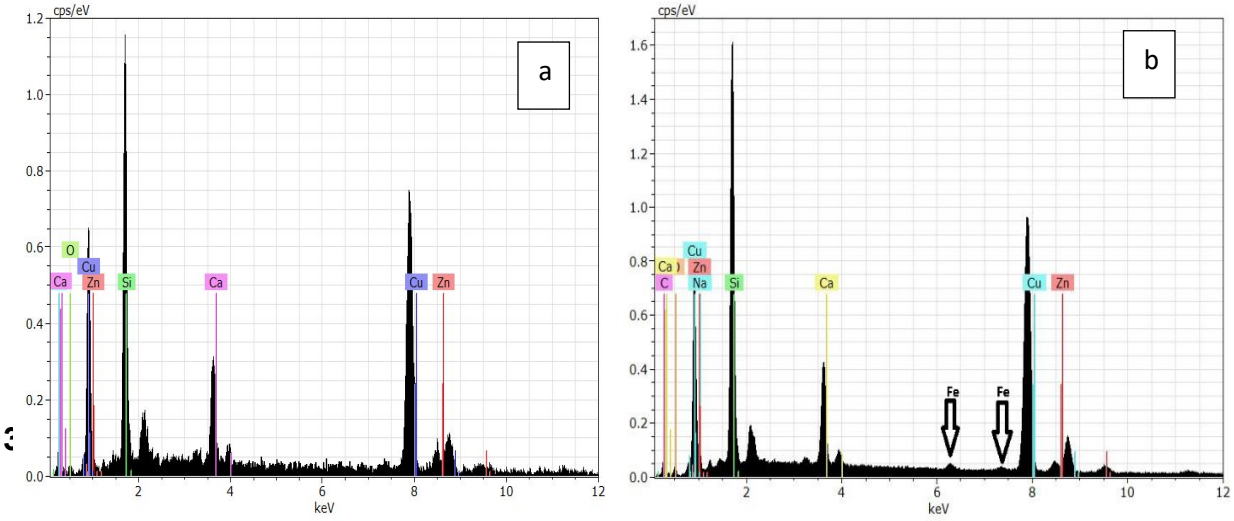

Fig.3: Energy Dispersive X-ray Spectroscopy of **a)** CuO:ZnO and **b)** Fe-doped CuO:ZnO thin films for 0.3 Fe content.

The UV–VIS–NIR spectrophotometer was employed to investigate the optical properties of the $(CuO: Zn)_{1-x}(Fe)_x$ thin films at room temperature. Figure 4 shows the variation in optical transmittance as a function of wavelength in the range of 340–1100 nm for the CuO: ZnO films doped with different Fe concentrations and deposited by the PLD technique. As illustrated in the Figure, the transmittance reached approximately 90% for the film with x = 0.1, but decreased to nearly 30% when the Fe content was increased to x = 0.5. This significant reduction in transmittance can be attributed to the formation of defect states within the band gap, which serve as additional absorption centres, as well as to modifications in the electronic structure that enhance photon absorption within the visible region. Additionally, Fe doping can influence the crystallinity and particle size of the samples, leading to enhanced light scattering and a further reduction in optical transmittance. These results are consistent with the findings reported by S. Sogan [24].

The absorption coefficient (α) was calculated using Eq. (4):

$$\alpha = 2.303A/t \quad (4)$$

Where A and t are the absorbance and film thickness, respectively.
Figure 5 presents the absorption coefficient (α) as a function of wavelength for the CuO: ZnO thin films doped with Fe (x = 0.1, 0.2, 0.3, 0.4, and 0.5). The absorption coefficient was determined by analyzing the high-absorption region near the fundamental absorption edge of the films. The results indicate that α increases progressively with increasing Fe concentration, reflecting enhanced light absorption. This behavior can be attributed to the formation of defect states and intermediate energy levels within the band gap, which facilitate electronic transitions between the valence and conduction bands. A distinct UV absorption band is observed around 340 nm in all films, while the absorbance stabilizes above 900 nm, illustrating the characteristic optical response of the Fe-doped sample.

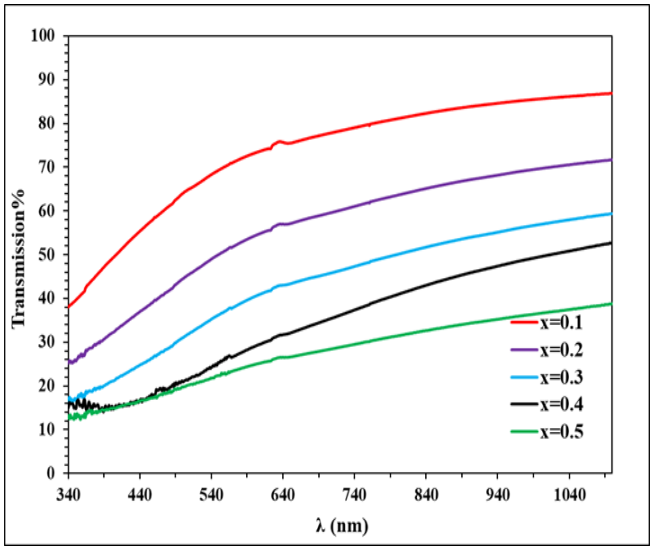

Fig.4: The variation of transmission with the wavelength for (CuO:Zn) -$_x$Fe$_x$ thin films with different concentrations of Fe.

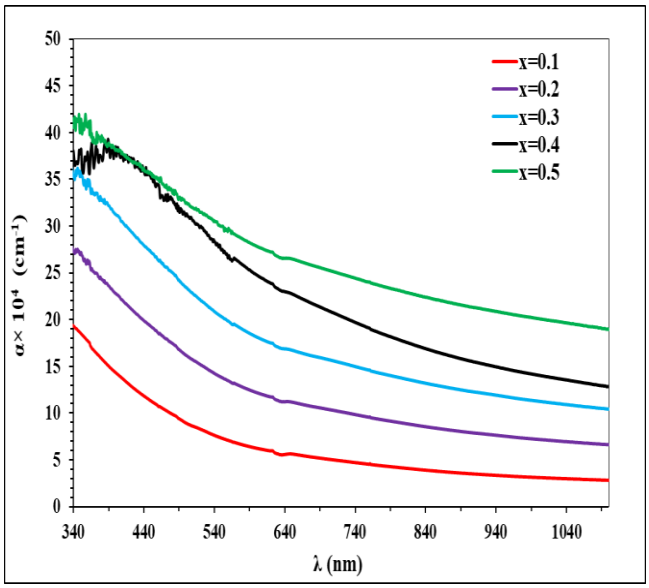

Fig.5: The absorption coefficient versus wavelength of $(CuO:Zn)_{1-x}(Fe)_x$ films prepared by PLD Technique.

The Tauc equation establishes a direct relationship between the absorption coefficient and the optical energy gap (E_g). In [25] Eq. (5),

$$(\alpha h\nu)^2 = B(h\nu - E_g) \quad (5)$$

The optical energy band gap (E_g) of the $(CuO: Zn)_{1-x}(Fe)_x$ thin films was determined using the Tauc method. In this approach, the photon energy (hν), absorption coefficient (α), Planck's constant (h), light frequency (ν), and the material-dependent parameter B—which is inversely related to amorphous content-are incorporated into the Tauc equation. The band gap was estimated by plotting $(\alpha h\nu)^2$ versus photon

energy (hν) and extrapolating the linear portion of the curve to α = 0, indicating direct allowed transitions, as shown in Figure 6.The results demonstrate that increasing Fe content leads to a progressive decrease in the optical band gap of the films. This reduction is attributed to the formation of defect states and localized energy levels within the band gap, which facilitate electronic transitions from the valence band to the conduction band, thereby lowering the energy required for these transitions. Consequently, higher Fe concentrations result in a narrower band gap and enhanced light absorption. These observations are in good agreement with previously reported studies [26, 27].

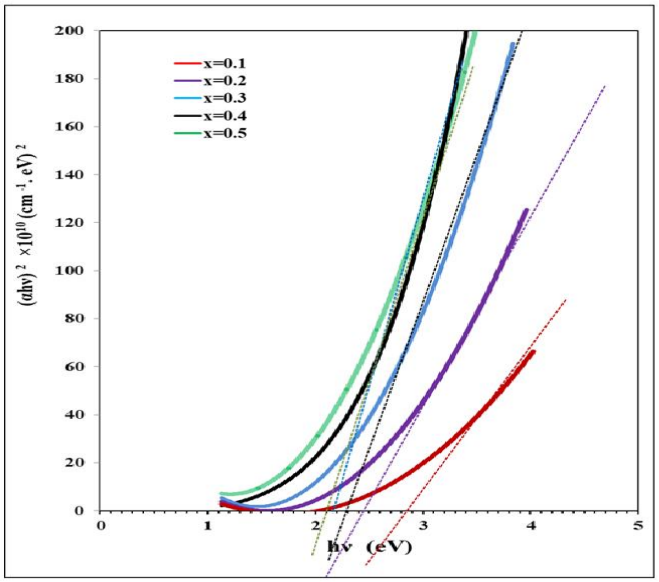

Fig.6: The Variation of (αhυ)2 with (hυ) for $(CuO:Zn)_{1-x}(Fe)_x$ thin films with different concentrations of Fe.

The refractive index (n) can be calculated from the reflectance coefficient r using Eq. (6) [28].

$$n = \text{sqrt}((1 + r) / (1 - r)) \quad (6)$$

The dependence of the refractive index on wavelength for the $(CuO: Zn)_{1-x}(Fe)_x$ thin films is presented in Figure 7.

In general, n increases with increasing wavelength, except for the films with x = 0.1 and x = 0.4. Furthermore, the refractive index decreases with the increasing Fe concentration, indicating a non-linear dependence of n on Fe doping. For low Fe concentrations (x = 0.1–0.3), n decreases with increasing wavelength because the limited number of localized defect states reduces electronic polarization.

At medium concentration (x = 0.4), n exhibits mixed behaviour, as the accumulation of defect states begins to enhance polarisation. At high concentration (x = 0.5), n increases significantly with wavelength, reflecting the pronounced influence of abundant localized states and enhanced electronic polarization. These observations are consistent with previous reports on CuO thin films prepared by the activated reactive evaporation technique, which exhibited similar refractive-index behavior [2]. The extinction coefficient was calculated using Eq. (7), [30]:

$$k = \frac{\alpha\lambda}{4\pi} \quad (7)$$

Figure 8 shows the variation of the extinction coefficient (k) as a function of wavelength for the $(CuO: Zn)_{1-x}(Fe)_x$ thin films at different Fe concentrations.

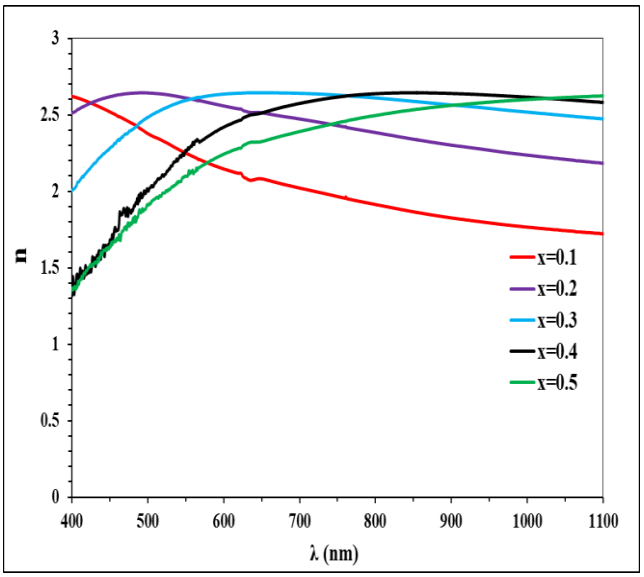

Fig.7: Variation of the refractive index (n) as a function of wavelength for $(CuO:Zn)_{1-x}(Fe)_x$ thin films with different Fe concentrations.

The results indicate that k increases progressively with increasing Fe content from x = 0.1 to 0.5. This behavior mirrors the trend observed for the absorption coefficient (α), suggesting that Fe incorporation enhances light absorption across the visible and near-infrared regions. The increase in k can be attributed to the formation of localized defect states within the lattice, which enhance electronic polarization and the interaction between light and the material. This progressive increase in k is consistent with the observed changes in refractive index, transmittance, and absorption, confirming that Fe doping effectively modifies the optical behavior of the films.

The real (εr) and imaginary (εi) parts of the dielectric constant were calculated using the following [30] relations:

$$\varepsilon r = n^2 - k^2 \quad (8)$$

$$\varepsilon i = 2nk \quad (9)$$

Figures 9 and 10 present the variations of the real (εr) and imaginary (εi) components of the dielectric constant as a function of wavelength for the $(CuO: Zn)_{1-x}(Fe)_x$ thin films with different Fe concentrations. Table 2 shows the variation in optical parameters with changes in the Fe content in the films. The film's dielectric behavior is strongly dependent on Fe content. At low Fe concentrations (x = 0.1), εr decreases while εi remains relatively high, indicating limited polarization and higher energy loss. For medium Fe concentrations (x = 0.2–0.3), εr stabilises and εi decreases gradually.

At high Fe concentrations (x = 0.4–0.5), εr increases while εi decreases, reflecting enhanced energy storage and reduced dielectric losses. These observations suggest that careful optimization of Fe content can improve the dielectric performance of CuO: ZnO films for applications in capacitors, sensors, and high-frequency devices.

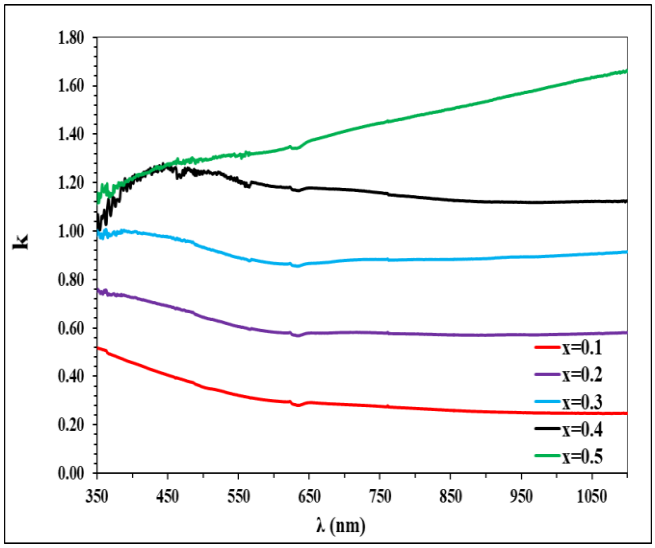

Fig.8: The variation of k with the wavelength for $(CuO:Zn)_{1-x}(Fe)_x$ thin films with different concentrations of Fe.

Table 2. Optical parameters of Fe-doped CuO: ZnO thin films.

Sample	A	T%	α (cm^{-1})	K	n	ε_r	ε_i	Eg (eV)
x=0.1	0.16	69.26	73466	0.322	2.250	4.959	1.448	2.90
x=0.2	0.30	50.04	138474	0.606	2.611	6.447	3.166	2.50
x=0.3	0.44	36.15	203482	0.891	2.594	5.934	4.623	2.30
x=0.4	0.60	25.36	274379	1.202	2.269	3.704	5.452	2.00
x=0.5	0.65	22.36	299601	1.312	2.100	2.690	5.511	2.00

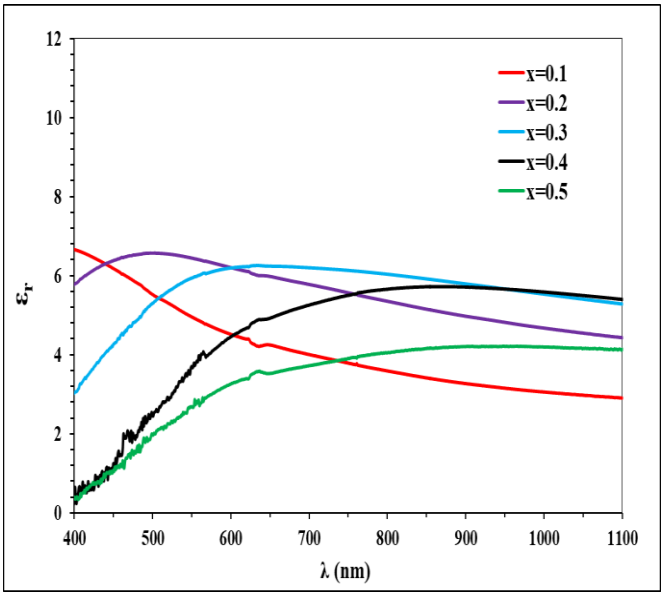

Fig.9: The variation of εr with the wavelength for $(CuO: Zn)_{1-x}(Fe)_x$ thin films with different concentrations of Fe.

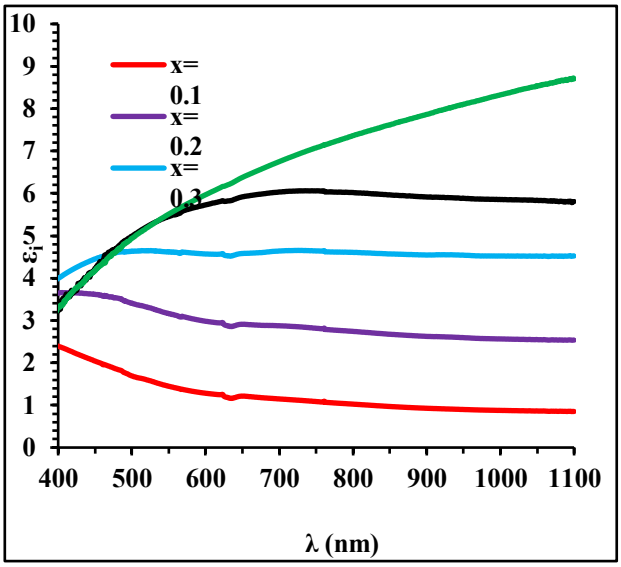

Fig.10: The variation of εi with the wavelength for $(CuO: Zn)_{1-x}(Fe)_x$ thin films with different concentrations of Fe.

4. Conclusions

Fe-doped $(CuO: Zn)_{1-x}(Fe)_x$ thin films with Fe concentrations ranging from 0.1 to 0.5% were successfully fabricated using the pulsed laser deposition (PLD) technique. The incorporation of Fe was found to significantly influence the structural, optical, and dielectric properties of the films. Specifically, Fe doping led to improved crystallinity, modified optical absorption and band gap, enhanced refractive index and extinction coefficient, and optimised dielectric behaviour. These enhancements demonstrate that Fe incorporation effectively tailors the material's performance, making the films up-and-coming for optoelectronic applications, including photovoltaic cells, optical sensors, capacitors, and high-frequency electronic devices.

References

[1] S. Siwatch, V. S. Kundu, A. Kumar, S. Kumar, N. Chauhan, & M. Kumari, "Morphology correlated efficiency of ZnO photoanode in dye sensitized solar cell," Materials Research Express, 6, 1050d3 (2019).
[2] A. S. Maktoof, G. H. Mohammed, & H. H. Abbas, "Effect of annealing process on structural and optical properties of Au-doped NiO: WO3 thin films fabricated by PLD technique," Applied Surface Science, 450, 123–130 (2022).
[3] Z. Kayani, S. Iram, R. Rafi, S. Riaz, & S. Naseem, "Effect of Cu doping on the structural, magnetic and optical properties of ZnO thin films," Applied Physics A, 124(7), 468 (2018).
[4] J. K. Wu, W. J. Chen, Y. H. Chang, Y. F. Chen, D. R. Hang, C. T. Liang, & J. Y. Lu, "Fabrication and photoresponse of ZnO nanowires/CuO coaxial heterojunction," Nanoscale Research Letters, 8, 387 (2013).
[5] M. Kawwam, F. H. Alharbi, T. Kayed, A. Aldwayyan, A. Alyamani, N. Tabet, & K. Lebbou, "Structural and optical properties of CuO thin films," Applied Surface Science, 276, 7–12 (2013).
[6] A. El-Trass, M. M. El-Khatib, A. M. Abdel-Ghany, & H. M. El-Shazly, "Structural and optical characterisation of copper oxide thin films prepared by chemical methods," Applied Surface Science, 258, 2997–3001 (2012).
[7] D. N. Jassim, J. M. Mansour, & G. H. Mohammed, "Influence of Mn2O3 concentrations on the structural and optical characterisation of ZnO: CuO thin films prepared by laser technique," Journal of Optics, (2024).
[8] S. Ghosh, P. Srivastava, B. Pandey, M. Saurav, P. Bharadwaj, D. Avasthi, D. Kabiraj, & S. Shivaprasad, "Study of ZnO and Ni-doped ZnO synthesised by atom beam sputtering technique," Materials Science and Engineering B,

90(4), 765–769 (2008).
[9] C. Gümüş, O. M. Ozkendir, H. Kavak, & Y. Ufuktepe, "Structural and optical properties of CuO thin films," Journal of Optoelectronics and Advanced Materials, 8(1), 299–303 (2006).
[10] M. Rusu, G. G. Rusu, M. Girtan, & S. Dabos Seignon, "Structural and optical characterisation of nanocrystalline CuO thin films," Journal of Non-Crystalline Solids, 345, 4461–4464 (2008).
[11] F. Zahra, et al., "Characterisation techniques of Fe-doped CuO thin films deposited by the spray pyrolysis method," arXiv preprint, arXiv:1807.09697 (2018).
[12] C. H. B. Ng & W. Y. Fan, "Optical properties of copper oxide thin films," Journal of Physical Chemistry B, 110, 20801–20806 (2006).
[13] V. Figueiredo, E. Elangovan, G. Goncalves, P. Barquinha, L. Pereira, N. Franco, E. Alves, R. Martins, & E. Fortunato, "Effect of post-annealing on the properties of copper oxide thin films obtained from the oxidation of evaporated metallic copper," Applied Surface Science, 254, 3949–3954 (2008).
[14] P. Samarasekara, N. T. R. N. Kumara, & N. U. S. Yapa, "Sputtered copper oxide (CuO) thin films for gas sensor devices," Journal of Physics: Condensed Matter, 18, 2417–2420 (2006).
[15] D. Jundale, S. Pawar, M. Chougule, P. Godse, S. Patil, B. Raut, S. Sen, & V. Patil, "Nanocrystalline CuO thin films for H2S monitoring: microstructural and optoelectronic characterisation," Journal of Sensor Technology, 1, 36–46 (2011).
[16] S. Sinthamani, M. Ranjithkumar, S. K. Bharatan, & S. Anitha, "Optical characterisation of RF sputtered copper oxide for thin film solar cell applications," Materials Today: Proceedings, 59,814–818 (2022).
[17] I. Singh & R. K. Bedi, "Studies and correlation among the structural, electrical and gas response properties of aerosol spray deposited self-assembled nanocrystalline CuO," Applied Surface Science, 257, 7592–7599 (2011).
[18] Borah, J., & Sarma, B. K. (2022). Structural, optical and electrical properties of CuO nanostructures prepared by reactive DC magnetron sputtering. Materials Today: Proceedings, 65, 2523-2528.
[19] Mohammed Enad, A., & Rzaij, J. M. (2025). Synthesis of CuO Thin Film Incorporated with Nanostructured Nd2O3 Deposited by Pulsed Laser Deposition for Ammonia Sensing Applications. Nano, 20(03), 2450113.
[20] Rakshit, S., Mondal, K. G., Jana, P. C., Kamilya, T., & Saha, S. (2023). Structural and optical properties of chemically synthesised copper oxide nanoparticles and their photocatalytic application. Journal of Materials Science: Materials in Electronics, 34(32), 2141.
[21] Enad, A. M., & Rzaij, J. M. (2025). Study on the Structural and Optical Properties of CuO Thin Films Mixed with La2O3 Deposited using Pulsed Laser Deposition for Future Optoelectronic and Gas Sensing Devices Applications. Samarra Journal of Pure and Applied Science, 7(2), 185-198.
[22] Enad, A. M., & Rzaij, J. M. (2024). Investigate the structural, morphological, and topographical characteristics of CuO thin films utilising a pulsed laser deposition method-Journal of Theoretical and Applied Physics, 18.
[23] A. B. Taha, M. S. Essa, and B. T. Chiad, "Study the effect of reaction time on preparation of iron oxide nanoparticles by hydrothermal technique," Materials Science Forum, vol. 1084, pp. 23–30, 2023.
[24] A. M. El Sayed, & M. Shaban, "Structural, optical and photocatalytic properties of Fe and (Co, Fe) co-doped copper oxide spin-coated films," Spectrochimica Acta Part A: Molecular and Biomolecular Spectroscopy, 149, 638–646 (2015).
[25] P. Rani, S. Kumar, & R. Singh, "Study of structural and optical properties of Fe-doped CuO nanoparticles," AIP Conference Proceedings, 1728(1), 057007 (2016).
[26] B. Balamurugan & B. R. Mehta, "Optical and structural properties of nanocrystalline copper oxide thin films prepared by activated reactive evaporation," Thin Solid Films, 396, 90–96 (2001).
[27] J. Pankove, Optical Processes in Semiconductors, Prentice-Hall, New Jersey, Vol. 92 (1971).
[28] E. Hecht, *Optics*, 4th ed., Addison-Wesley, San Francisco, pp. 1–690 (2002).
[29] Nesa, M. (2016). Characterisation of zinc-doped copper oxide thin films synthesised by the spray pyrolysis technique.
[30] Palik, E. D. (1991). Optical properties of solids.

تأثير التطعيم بالحديد على بعض الخصائص التركيبية والبصرية لأغشية (CuO:ZnO) الرقيقة المحضرة بتقنية الترسيب بالليزر النبضي

رسل ربيع عبدالوهاب*، غصون حميد محمد

قسم علوم الفيزياء, كلية العلوم,جامعة بغداد, بغداد,العراق.

البريد الالكتروني للباحث:Rusul.Abd2404m@sc.uobaghdad.edu.iq

الخلاصة: تمت دراسة الخصائص التركيبية والبصرية لأغشية CuO:ZnO الرقيقة المشوبة بالحديد (Fe) بتراكيز مختلفة من 0.1 الى 0.5% والمترسبة على ركائز زجاجية باستخدام تقنية الترسيب بالليزر النبضي (PLD) عند درجة حرارة الغرفة وتحت ضغط فراغي مقداره 1×10^{-2}ملي بار. أظهرت نتائج حيود الأشعة السينية (XRD) أن جميع الأغشية احتفظت ببنيتها متعددة التبلور ذات الطور الاحادي، في حين انخفض الحجم الحبيبي مع زيادة تركيز الحديد. كما أكد تحليل مطيافية تشتت الطاقة للأشعة السينية (EDS) نجاح دمج عنصر الحديد دون التأثير على نسب عنصري النحاس والزنك. وقد تبين أن زيادة تركيز الحديد تؤثر بشكل ملحوظ في النفاذية البصرية والامتصاص ومعامل الانكسار (n) ومعامل الخمود (k) والثوابت العازلة، مما يدل على أن التشويب بالحديد يحدث تغييرا جوهريا في الخصائص التركيبية والبصرية والعازلية لأغشية CuO:ZnO الرقيقة.